Synthesis and characterization of polymer nanocomposites from methyl acrylate and metal chloride and their application

Zainab A. Abdul Latif, Ahmed Mishaal Mohammed & Nada M. Abbass

Springer

Springer

ORIGINAL PAPER

Synthesis and characterization of polymer nanocomposites from methyl acrylate and metal chloride and their application

Zainab A. Abdul Latif[1] · Ahmed Mishaal Mohammed[1] · Nada M. Abbass[2]

Abstract

This work involved the preparation of nanoparticles for Fe_3O_4 oxides with $NiCl_2$ and $V_2O_5SO_4$ by using ferric chloride as a mineral salt. X-ray diffraction (XRD), atomic force microscopy (AFM), scanning electronic microscopy (SEM), field emission scanning electronic microscopy, Fourier transform infrared spectroscopy, thermogravimetry analysis and differential scanning calorimetric (DSC) analysis were performed. The efficiencies of NiO and V_2O_5 were measured for gas sensitivity and light detection, which were high in both analyses. AFM tests showed that different nanoparticles formed similar acrylate polymers to NiO and V_2O_5 with the diameters ranging from 72.12 to 88.12 nm. The XRD measurements showed the hexagonal shape of NiO, while the axon axes were observed for V_2O_5 in SEM measurements. The image measurements showed different forms of polymer compositions. Moreover, the thermodynamic analysis indicated a thermal dissolution for both polymers and oxides prepared at extremely high temperatures. Finally, DSC tests identified the effect of polymer filled with oxide and its comparison with pure polymer.

Keywords Polymer composites · Methyl acrylate · Gas sensor · XRD

Introduction

Nanotechnology is the process occurring in connection with physics, chemistry, and biology [1, 2]. As defined by size, nanotechnology is also naturally extremely broad, thereby counting the diverse fields of science [3], such as organic chemistry, surface science, molecular biology, semiconductor physics [4, 5], micro-fabrication [6],

✉ Ahmed Mishaal Mohammed
sc.dr.ahmedm.mohammed@uoanbar.edu.iq

1 Department of Chemistry, College of Science, University Of Anbar, Ramadi, Iraq

2 Department of Chemistry, College of Science, University of Baghdad, Baghdad, Iraq

and molecular engineering [7]. Nanosensors that detect gases are generally based on metal oxides or conducting particles.

Conducting polymer nanocomposites (i.e., conducting particles embedded into an insulating polymer matrix) can quantify and/or identify microorganisms on the basis of their gas emissions and are also extremely important because of their electrical, electronic, magnetic and optical properties, which are related to their conjugated π electron backbones [8–10]. Polymer nanocomposites containing surface-engineered metal oxides continuously offer new opportunities to enhance desired properties or functionalities, such as optical transparency, ductility, flexibility, and molecular mobility [11]. To prevent the agglomeration of these inorganic metal oxides in organic polymer matrix, researchers adopted various functional methods, including the use of surfactants [12] and silane coupling agents [13].

Sol–gel method has gained attention as a promising method for nanomaterial synthesis due to its mild reaction conditions and building up the materials from molecular precursors, thereby leading to variation in materials and properties [14]. The resulting product of sol–gel method is either films or colloidal powders. The sol–gel method can produce micro- and nanostructures. The size, shape, and structure of final products are considerably influenced by the reaction parameters [15]. The purpose of this paper was to synthesize of new inorganic polymer nanocomposites to increase the properties of polymer such as heat resistance, mechanical strength, and impact resistance and decrease other properties, such as electrical conductivity and dielectric constant, by increasing their permeability for gases and applications on the prepared nanocomposites including gas sensor.

Materials and methods

Chemicals

Deionized distilled water was used to prepare all the solutions. $NiCl_2 \cdot 6H_2O$, $VOSO_4 \cdot 4H_2O$, and methyl acrylate $C_4H_6O_2$ were commercially obtained from Sigma-Aldrich. The analytical grade of this study was based on all involved chemicals and reagents.

General experimental methods

Standard solution preparation

The aqueous solution of methyl acrylate (MA) (MA/water 7:3) and 5% ammonium per sulfate solution were prepared for the experiment. The standard solution was prepared by dissolving stoichiometric amounts of the metal salts in distilled water. Then, NaOH solution was standardized against a solution of oxalic acid as a primary standard solution and titrated as dibasic acid (25 ml) of oxalic acid. Five drops of phenolphthalein were also titrated with the NaOH solution. Phenolphthalein is often

neutralized compared with other acids. A stable pink color appeared, and the solution was stirred often until the last drop of NaOH was added.
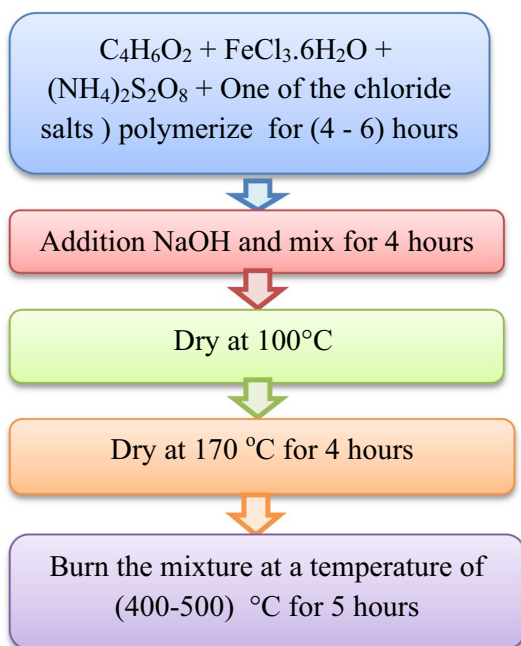
Composite synthesis

The composite was prepared according to a method described by Singh and Birendra [16]. As illustrated in Scheme 1, ferric chloride solution (10 ml, 0.1 N, 0.135 g) was added to 10 ml of MA solution (MA:water: 7:3) by stirring. A 5% $(NH_4)_2S_2O_8$ and 5 ml of the salts of one element used were added to the NaOH solution (2.6 ml, 1 N, 2 g) at the temperature ranging from 70 to 90 °C, and the solution was stirred for 4 h. The solution was dried to yield poly-MA, which was dried at the temperature ranging from 90 to 100 °C overnight. The resulting mixture was heated at 170 °C for approximately 3 h to obtain the amorphous nature of salt. The last salts were heated at the temperature ranging from 400 to 500 °C for 5 h in air, then quietly cooled, and collected until use.

Material characterization

X-ray diffraction (XRD) spectra of samples were measured using an automated diffract meter Shimadzu 6000 XRD, and Cu-Kα radiation ($\lambda = 1.5418$ Å) was conducted to investigate the sample phase composition and crystalline properties. The surface morphology quality and elemental composition quantity were analyzed through scanning electron microscopy (SEM), field emission SEM

Scheme 1 Synthesis of composite

$C_4H_6O_2$ + FeCl$_3$.6H$_2$O + $(NH_4)_2S_2O_8$ + One of the chloride salts) polymerize for (4 - 6) hours

⬇

Addition NaOH and mix for 4 hours

⬇

Dry at 100°C

⬇

Dry at 170 °C for 4 hours

⬇

Burn the mixture at a temperature of (400-500) °C for 5 hours

(FE-SEM), and atomic force microscopy (AFM) SPM-AA3000 of Angstrom Advanced Inc., USA, using AFM contact mode. The chemical functional groups of the sample that did not undergo annealing were characterized through Fourier transform infrared spectroscopy (FTIR) Shimadzu FTIR-8400S/KBr which was identified by wave number ranging from 400 to 4000 cm^{-1}. The DSC analysis was performed to measure the lines by using STA PT-1000 differential scanning calorimetry. Thermogravimetry analysis (TGA) was conducted using mettle TA4000 system thermobalance at a heating rate of 10 °C/min, and it was used as the inert gas.

Physical applications

Thin film preparation

The thin films of V_2O_5, NiO, and methyl acrylate were prepared using the spin-coating method by using the prepared gel. The compound was prepared by combination of iron (III) chloride with ammonium thiosulphate and chloride one of the salts used with the acrylate in the same proportions used in the first preparation method prepared with distilled water and then polymerized 2 h on a magnetic stirrer with 500 RDM and 1 min. The prepared films were incubated with 500 °C for 5 h [17].
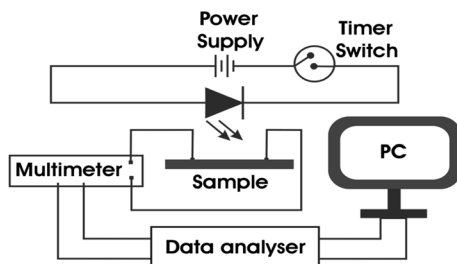
Light detection

The prepared V_2O_5/MA and NiO/MA thin films were tested for UV light sensing by using the provided setup system as shown in Fig. 1.

The 320 nm UV LEDs were employed as sources of light for 20 s (off–on). The UV sensitivity of the prepared films was defined using the following equation:

$$S = \frac{I_{UV} - I_{dark}}{I_{dark}} \tag{1}$$

Fig. 1 A scheme of photodetector test system

where I_{UV} is the measured current with UV in light exposure and I_{dark} is the measured current in the dark.

Gas sensing

V_2O_5/MA and NiO/MA thin films were also examined for N_2 sensing using the given system (Fig. 2).

The sensing properties were recorded under the atmospheric air conditions of N_2 gas at 10 °C, 20 °C, 30 °C, and 40 °C by measuring the electrical resistance (ER) of the tested films. The gas sensitivity formula was defined as follows:

$$S = \frac{R_g - R_a}{R_a} \times 100\% \tag{2}$$

where R_g and R_a are the film resistance in gas and air atmospheres, respectively. The response and recovery times were recorded by taking 90% of the maximum and minimum ERs of films, respectively [18].

Results and discussion

XRD

The XRD patterns of the prepared polymer nanocomposite powder are illustrated in Figs. 3 and 4. Figure 3 displays the XRD pattern for V_2O_5 powder prepared by using the sol–gel technique compared to ICDD card no. 96-901-2221 as a standard reference of orth. V_2O_5. The diffraction peaks located at $2\Theta = 21.3547°$, 25.6285°, 26.3827°, 33.0028°, 47.4581°, 52.4002° were indexed to (110), (210), (101), (301), (020), (600), (021), (420), (611) and (412) planes, respectively. These planes were observed confirming the orthorhombic structure for V_2O_5. The peaks corresponding to cubic Fe_2O_3 were also observed in all samples, as shown in Table 1.

Figure 4 reveals the XRD pattern for Cub. NiO compared to ICDD no. 96-900-8694 as a standard reference. The diffraction peaks indexed to (111), (200), and (220) planes are shown in Tables 2, 3, 4, and 5). Cub. NiO showed

Fig. 2 Sensing system used to record the sensing properties of the prepared films
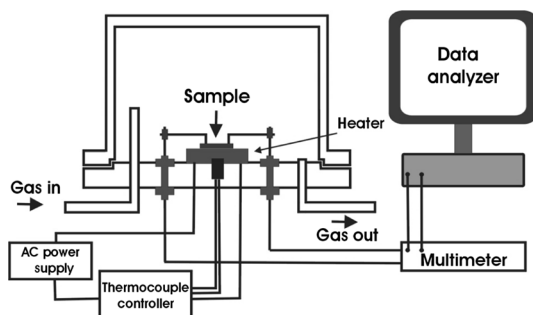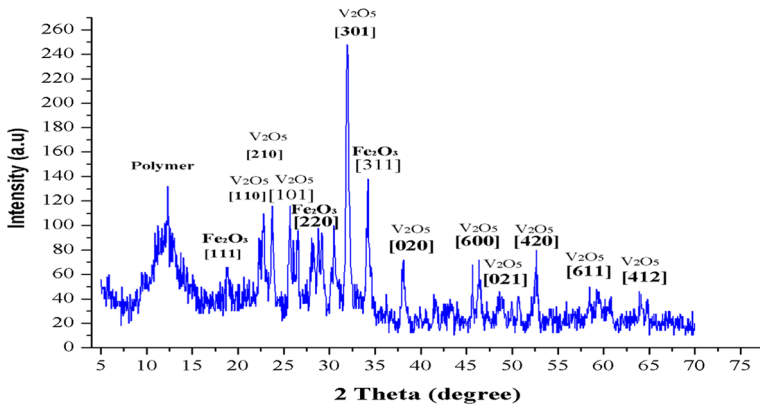
Fig. 3 X-ray diffraction pattern of PMA/VONC compared to standard V_2O_5 (ICDD no. 96-901-2221)
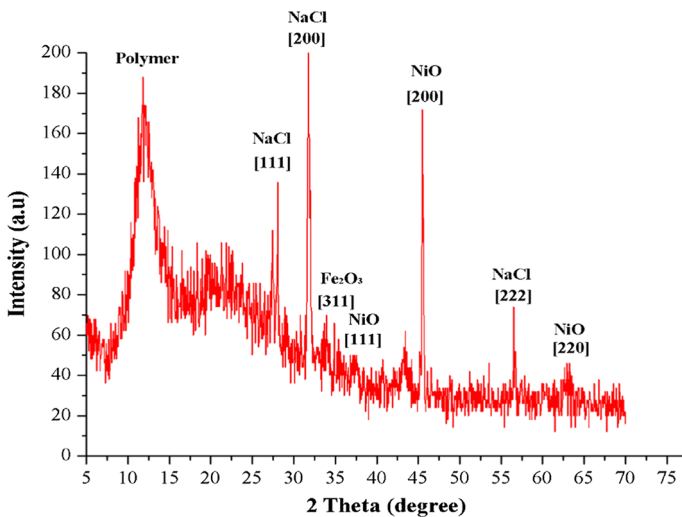

Fig. 4 X-ray diffraction pattern of PMA/NiONC compared to standard NiO (ICDD no. 96-900-8694)

that the peaks at $2\Theta = 37.2881°$, $43.4322°$, and $62.9661°$ were attributed to (111), (200), and (220) of (Cub. NiO) planes, respectively (Table 4).

SEM

In SEM micrographs, the morphology and particle size distribution of these polymer nanomaterials obtained by sol–gel method are indicated in Figs. 5 and 6. The morphology of the samples showed the presence of polymer compositions in different forms.

Table 1 Structural parameters of PMA/VONC as obtained from XRD analysis

2Θ (°)	FWHM (°)	d_{hkl} Exp. (A°)	G.S (nm)	d_{hkl} Std. (A°)	hkl	Phase	Card no.
18.7570	0.3352	4.7271	24.0	4.8093	(111)	Cub. Fe_2O_3	96-900-6317
21.3547	0.2932	4.1575	27.6	4.0976	(110)	Orth. V_2O_5	96-901-2221
25.6285	0.3352	3.4731	24.3	3.4907	(210)	Orth. V_2O_5	96-901-2221
26.3827	0.2514	3.3755	32.5	3.4115	(101)	Orth. V_2O_5	96-901-2221
30.7402	0.5028	2.9062	16.4	2.9451	(220)	Cub. Fe_2O_3	96-900-6317
33.0028	0.4190	2.7120	19.8	2.6175	(301)	Orth. V_2O_5	96-901-2221
35.6844	0.2933	2.5141	28.5	2.5116	(311)	Cub. Fe_2O_3	96-900-6317
41.5084	0.3771	2.1738	22.5	2.1915	(020)	Orth. V_2O_5	96-901-2221
47.4581	0.5866	1.9142	14.8	1.9240	(600)	Orth. V_2O_5	96-901-2221
48.7570	0.4609	1.8662	18.9	1.8678	(021)	Orth. V_2O_5	96-901-2221
52.4022	0.7542	1.7446	11.7	1.7453	(420)	Orth. V_2O_5	96-901-2221
59.4832	0.5028	1.5527	18.2	1.5799	(611)	Orth. V_2O_5	96-901-2221
60.5726	0.4609	1.5274	20.0	1.5435	(710)	Orth. V_2O_5	96-901-2221
65.0140	0.4609	1.4334	20.4	1.4347	(412)	Orth. V_2O_5	96-901-2221

Table 2 Crystallographic data and refinement parameters for V_2O_5

Phase classification					
Name					
Mineral Name	Shcherbinaite				
Formula	$V_2\,O_5$				
I/Ic					
Sample Name	C (calculated)				
Quality					
Crystal structure					
Crystallographic data					
Space group	P m n 21 (31)				
Crystal system	orthorhombic				
Cell parameters	a = 11.5440 Å	b = 4.3830 Å	c = 3.5710 Å		
Atom coordinates	Element	Oxidation	*x*	*y*	*z*
	V	$^+5$	0.149	0.391	0
	O	-2	0.146	0.03	0.03
	O	-2	0.319	0.503	0.005
	O	-2	0	0.499	0.003

$a \neq b \neq c$
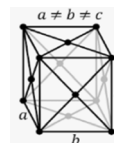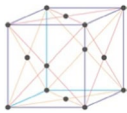
Table 3 Crystallographic data and refinement parameters for NiO

Phase classification	
Mineral Name	**Bunsenit**
Formula I/Ic	**NiO**
Sample Name **Quality**	**C** **(calculated)**

	Crystal structure
Crystallographic data	
Space group	**F m -3 m (225)**
Crystal system	**Cubic**
Cell parameters	**a = 4.1684 Å**
	a=b=c

Atom coordinates	**Element**	**Oxid.**	*x*	*y*	*z*
	Ni	**$^{+}2$**	**0**	**0**	**0**
	O	**$^{-}2$**	**0.5**	**0.5**	**0.5**

Table 4 Structural parameters of PMA/NiONC as obtained from XRD analysis

$2\varTheta$ (°)	FWHM (°)	d_{hkl} Exp. (A°)	G.S (nm)	d_{hkl} Std. (A°)	hkl	Phase	Card no.
27.4576	0.3813	3.2457	21.4	3.2566	(111)	Cub. NaCl	96-900-8679
31.8220	0.2966	2.8098	27.9	2.8203	(200)	Cub. NaCl	96-900-8679
35.3390	0.7627	2.5378	10.9	2.5116	(311)	Cub. Fe_2O_3	96-900-6317
37.2880	0.7627	2.4095	11.0	2.4066	(111)	Cub. NiO	96-900-8694
43.4322	0.5509	2.0818	15.5	2.0842	(200)	Cub. NiO	96-900-8694
45.5085	0.2966	1.9916	29.0	1.9942	(220)	Cub. NaCl	96-900-8679
56.5254	0.2966	1.6268	30.4	1.6283	(222)	Cub. NaCl	96-900-8679
62.9661	0.7627	1.4750	12.2	1.4738	(220)	Cub. NiO	96-900-8694

FE-SEM

The FE-SEM technique was utilized to observe the surface physical morphology for both PMA/VONC and PMA/NiONC. As indicated in Figs. 7 and 8, different forms were determined in PMA/VONC and PMA/NiONC, respectively. Moreover, interesting typical features such as ball- and tube-like structures have been observed for both PMA/VONC and PMA/NiONC, respectively.

Table 5 Crystallographic data and refinement parameters for Fe_2O_3

Phase classification					
Mineral Nam	**Maghemite**				
Formula I/I	**Fe_2O_3**				
Sample Name **Quality**	**C** **(calculated)**				
Crystal structure					
Crystallographic data					
Space group	**F d -3 m (227)**				
Crystal system	**Cubic**				
Cell parameters	**a = 8.3300 Å**				**a=b=c**
Atom coordinates	**Element**	**Oxid.**	***x***	***y***	***z***
	Fe	**$^{+}3$**	**0.5**	**0.5**	**0.5**
	Fe	**$^{+}3$**	**0.125**	**0.125**	**0.125**
	O	**–2**	**0.25**	**0.25**	**0.25**
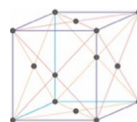
AFM

The AFM measurement was performed to determine the morphology of the prepared polymers (PMA/VONC and PMA/NiONC). The practical determination was based on the size in formation (length, width, and height) and other properties, such as surface texture and morphological characterization [18].

The PMA/VONC and PMA/NiONC images in Figs. 9 and 10 indicated a small particle size distribution with the diameters of 88.12 and 72.12 nm. All results concerning the AFM analysis matched the data obtained by XRD on the basis of the changes made in the volume fraction of all prepared composites.

FTIR

FTIR was used to reveal the incorporated nanometal oxides in the structure of the filled PMA materials. Figures 11 and 12 show the FTIR spectra of PMA/VONC and PMA/NiONC by using the wave number range of 400–4000 cm^{-1}.
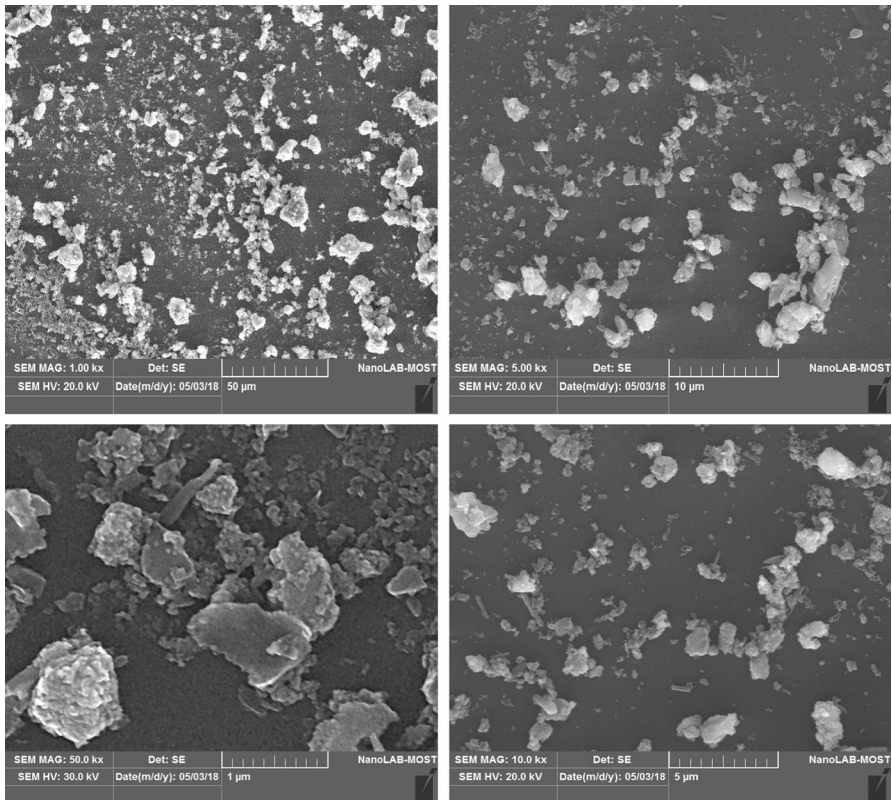
Fig. 5 SEM micrograph of nano-V_2O_5 synthesized in different magnifications

The spectra of all calcined samples showed two principal absorption bands in the region of 400–600 cm^{-1}. The vibration bands of both Fe–O and M–O corresponded to the substantial lattice vibration of the octahedral and tetrahedral coordination compounds in the spinel structure [19].

The bands observed at 617–621 cm^{-1} are the characteristics of an asymmetry stretching mode of the single-phase spin of structures [20]. Meanwhile, two other bands at 670–877 cm^{-1} are assigned to the bending modes of C–O and C–C aliphatic.

The bands observed at 2942 cm^{-1} are the characteristics of the asymmetry stretching mode of CH_2 group. As shown in Figs. 11 and 12, some bands corresponded to the characteristic adsorption of PMA chain, such as 1384–1440 (v C–C) and 1137–1445 cm^{-1} (δ C–H) vibrations from the methylene group. Bands appeared at 3400–3500 cm^{-1}, which belong to the O–H band of moisture [21]. The vibrational spectra of the absorption bands of the v Fe–O nanoparticles in PMA/VONC and PMA/NiONC were spotted at 511, 435, 482, 447, and 443 cm^{-1}. Other bands appeared at 465–621 cm^{-1}, which confirmed the formation of single-phase spinal structures [22].
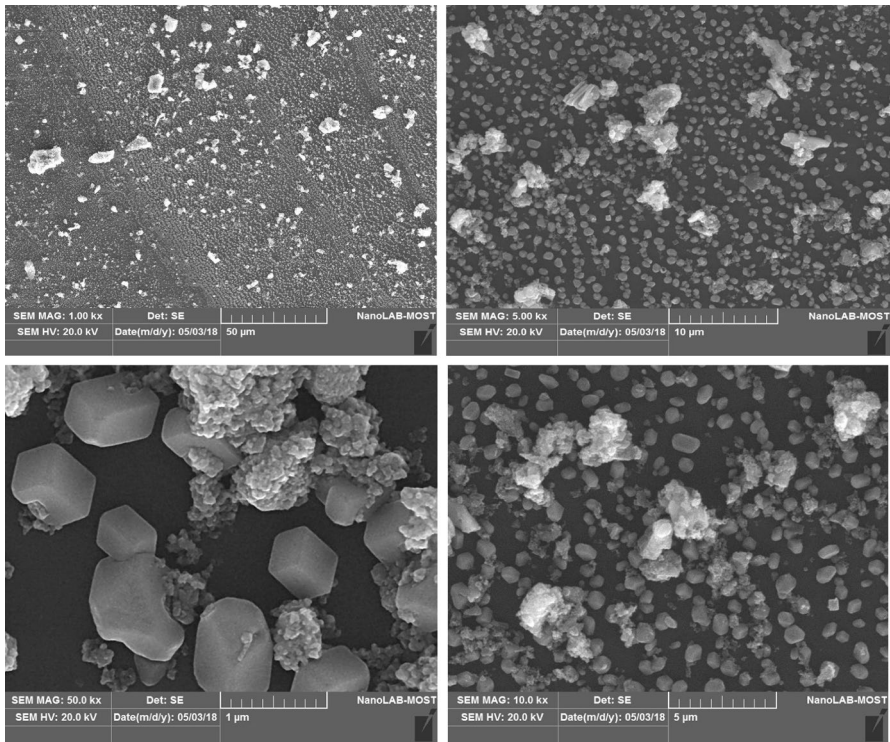
Fig. 6 SEM micrograph of nano-NiO synthesized in different magnifications
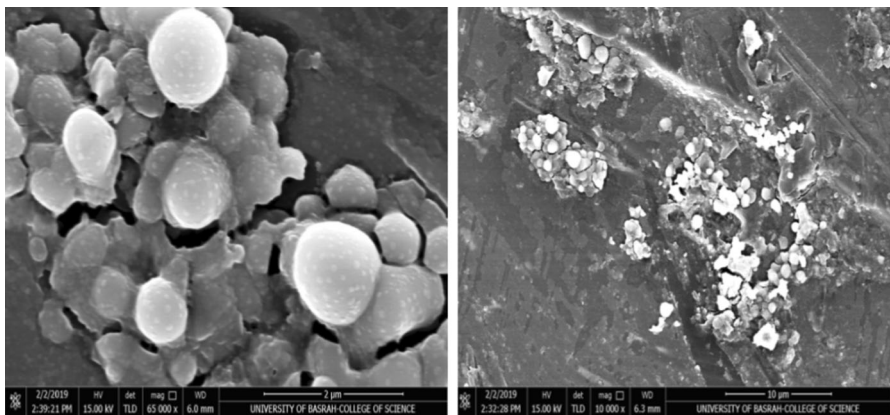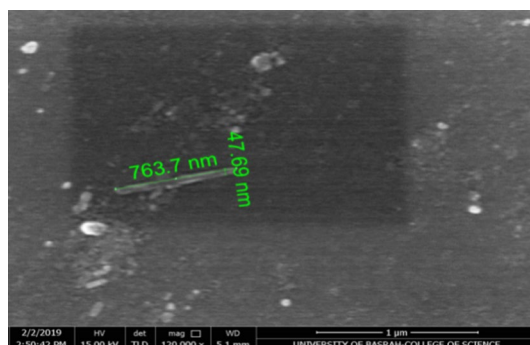

Fig. 7 FE-SEM for PMA/VONC

Accordingly, the appearance of the characteristic bonds for all polymers in FTIR spectra indicated that PMA chains were grafted onto the metal oxide surface during the polymerization process (Table 6).

Fig. 8 FE-SEM for PMA/NiONC

TGA, DTG, and DSC analyses for fallen and nanocomposite compounds

Figures 13 and 14 demonstrate the comparison between the thermogravimetry analysis (TGA) and differential scanning calorimetric (DSC) analysis of polymer nanocomposites, which were modified with VO^{+2} and Ni(II), respectively. Increasing the amount of organic matter was clearly visible in TGA. In contrast, a sharp degradation peak at low temperature was observed in the DSC thermograms, suggesting that this effect may be due to the small amount of MA modification present as a pseudo-bilayer but unbound as an ionic ally to the polymer surface. Figures 13 and 14 also illustrate the systems formed into a composite with vol.% fallen content. The thermal behavior of nanocomposites and the synergy among composite components were clearly visible as the thermal degradation of composites begins at a higher temperature than that of components [21, 23].

DSC analysis was performed to determine the thermal energy released via the chemical reactions of the polymers with metal chlorides during heating, which leads to exothermic and endothermic reactions. Endothermic reactions provided information on sample melting, phase transition, evaporation, dehydration, and pyrolysis. By contrast, exothermic reactions produce information on crystallization, oxidation, combustion, decomposition, and chemical reaction [24].

Figure 13 reveals that in the temperature ranging from 80 to 120 °C, the broad endothermic peaks were observed for both samples, which corresponded to the evaporation of absorbed water by polymer nanocomposites [25].

Light detection

Figure 15 illustrates the behavior of the photocurrent of both V_2O_5/PMA and NiO/PMA thin films with applied light.

The average sensitivity values of both V_2O_5/PMA and NiO/PMA thin films were 252.3% and 201.13%, respectively. The response and recovery time are listed in Table 7.
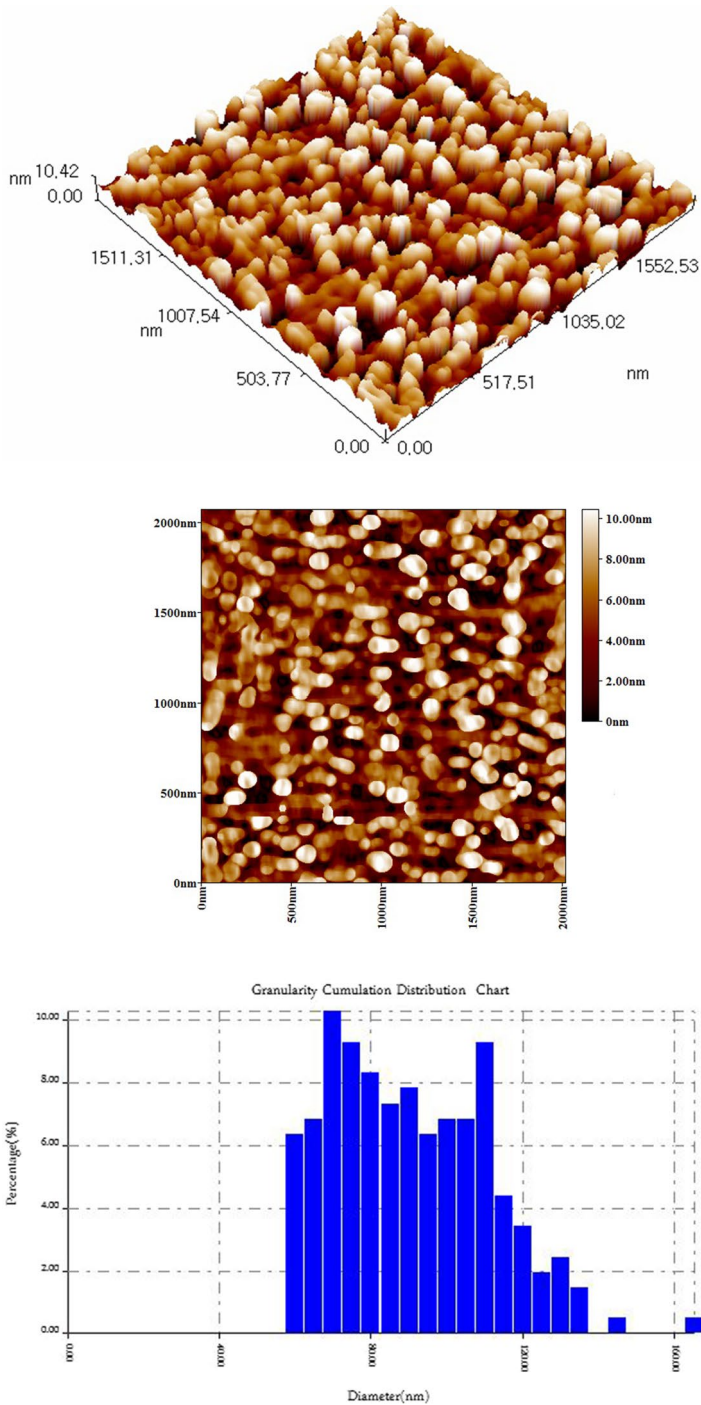
Fig. 9 AFM of two-dimensional and three-dimensional of PMA/VONC, the average distribution of diameter 88.12 nm
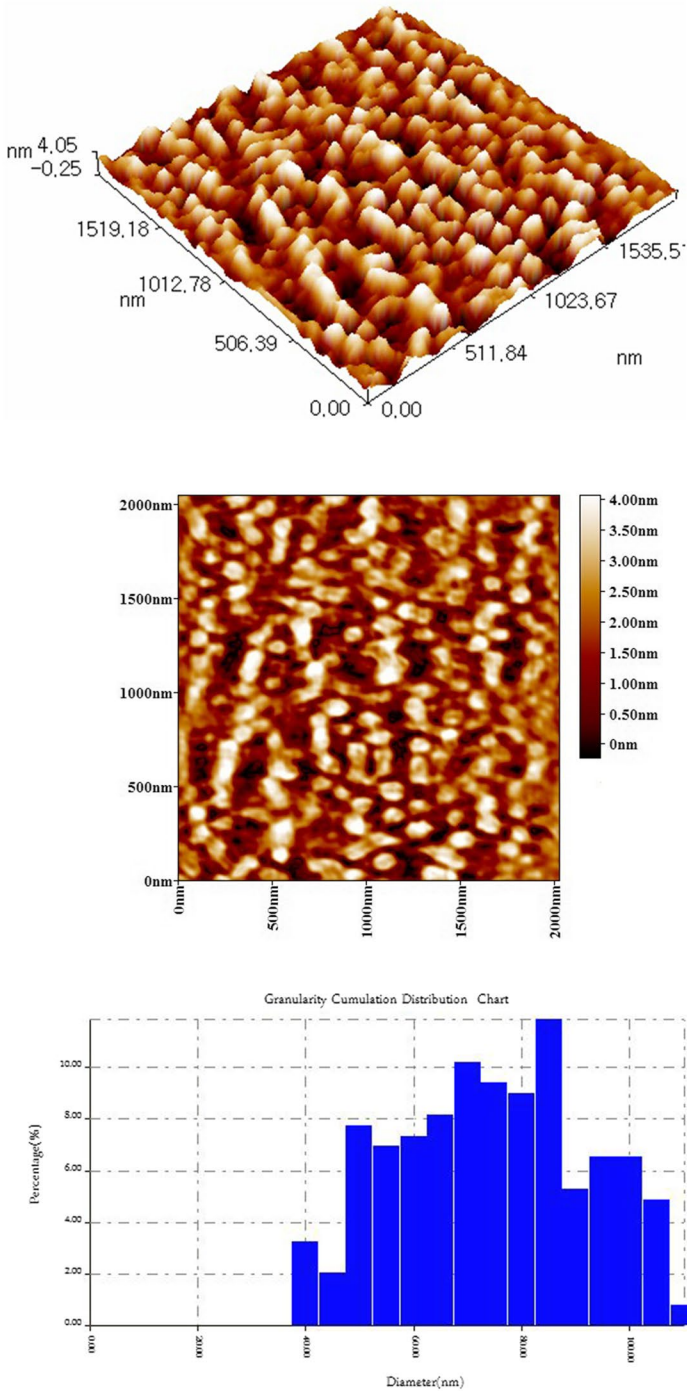
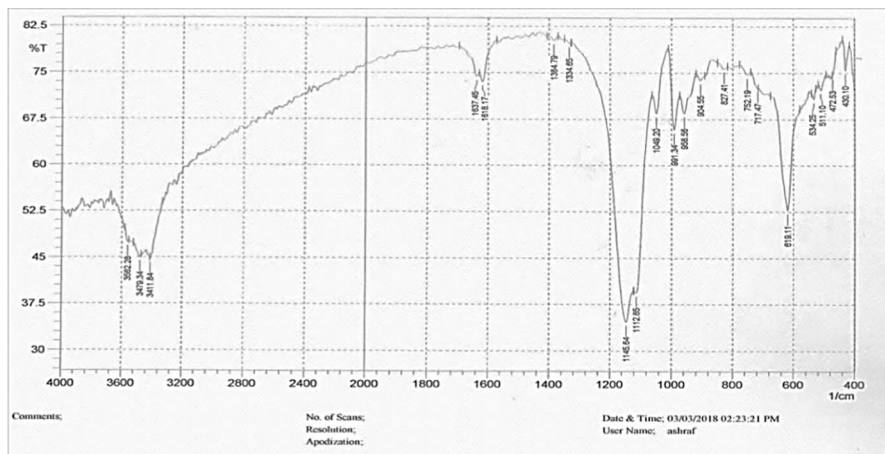**Fig. 10** AFM of two-dimensional and three-dimensional of PMA/NiONC, the average distribution of diameter 72.12 nm
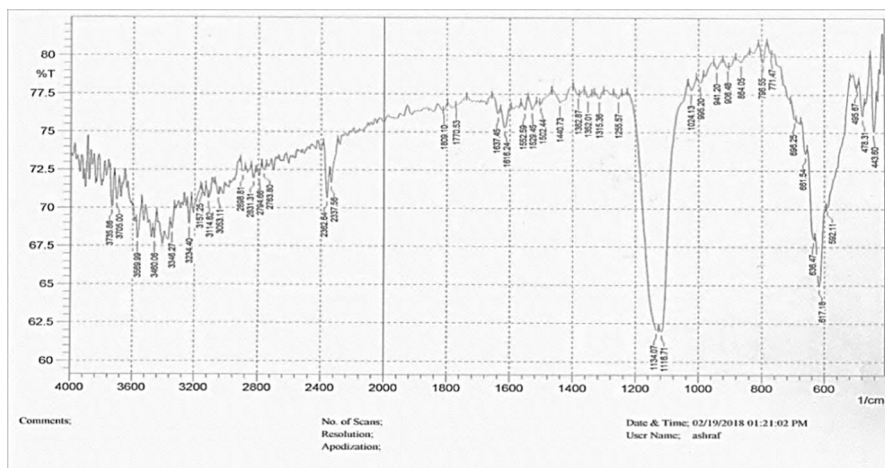
Fig. 11 FTIR spectrum of compound PMA/VONC

Fig. 12 FTIR spectrum of compound PMA/NiONC

Table 6 FTIR spectra of compounds

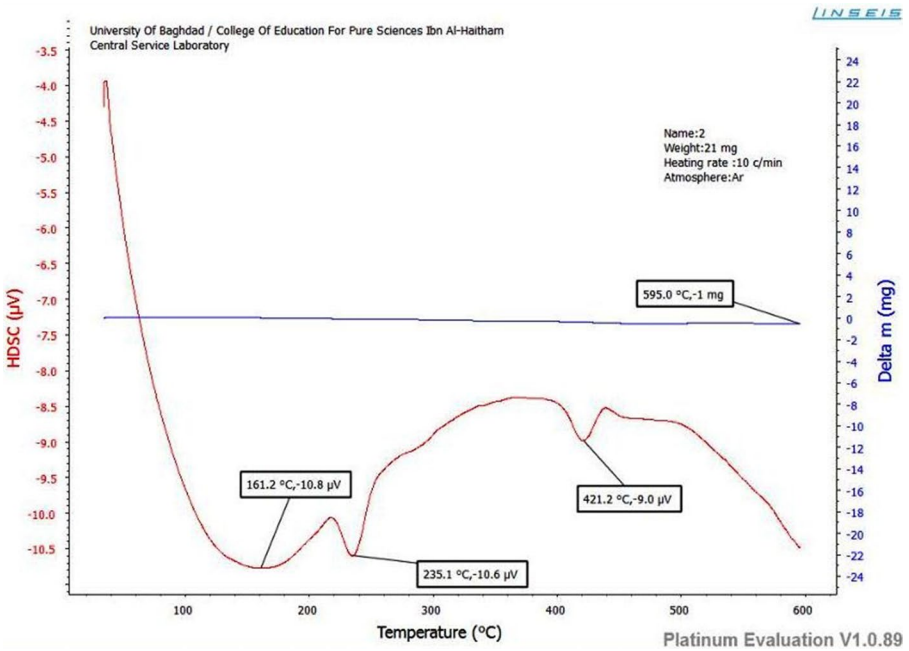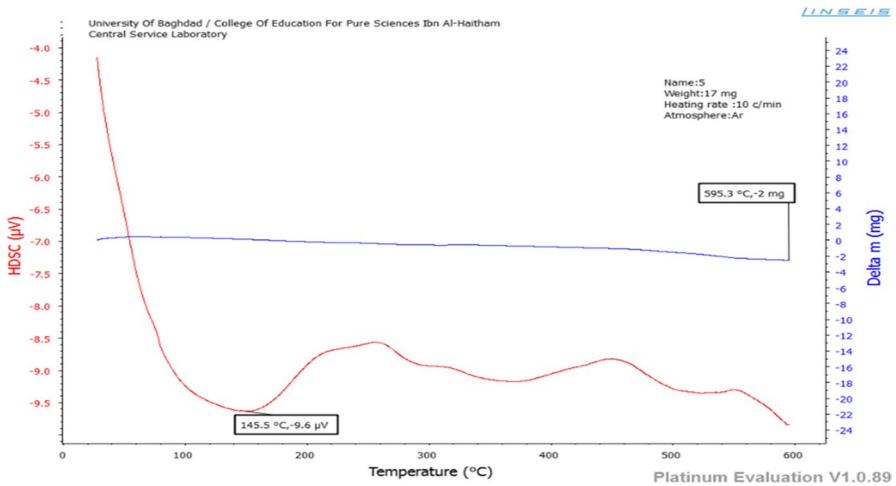| Compounds symmetric	Wave numbers of absorption band (cm^{-1})		
	v (C–C)	v (C–O)	Single-phase spinal structure
PMA/VONC	1384	1145	619
PMA/NiONC	1440	1134	617

Fig. 13 TGA/DTG curves of PMA/VONC

Fig. 14 TGA/DTG curves of PMA/NiONC

Gas sensing

Figures 16 and 17 illustrate the ER changing patterns of the tested films for both V_2O_5/PMA and NiO-PAM at 10 °C, 20 °C, 30 °C, and 40 °C. The exposure time
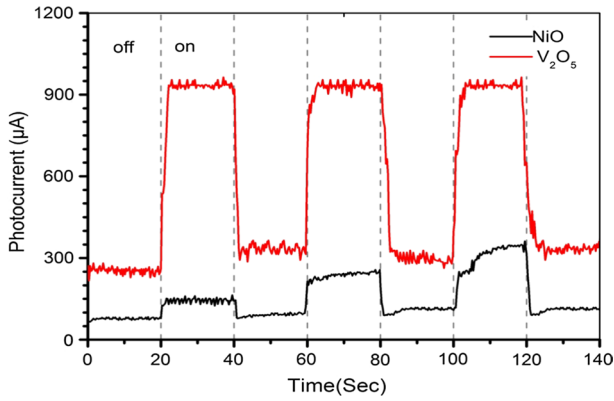
Fig. 15 Photodetectors of V_2O_5 and NiO

Table 7 Response and recovery times of the prepared V_2O_5/MA and NiO/MA thin films for UV light

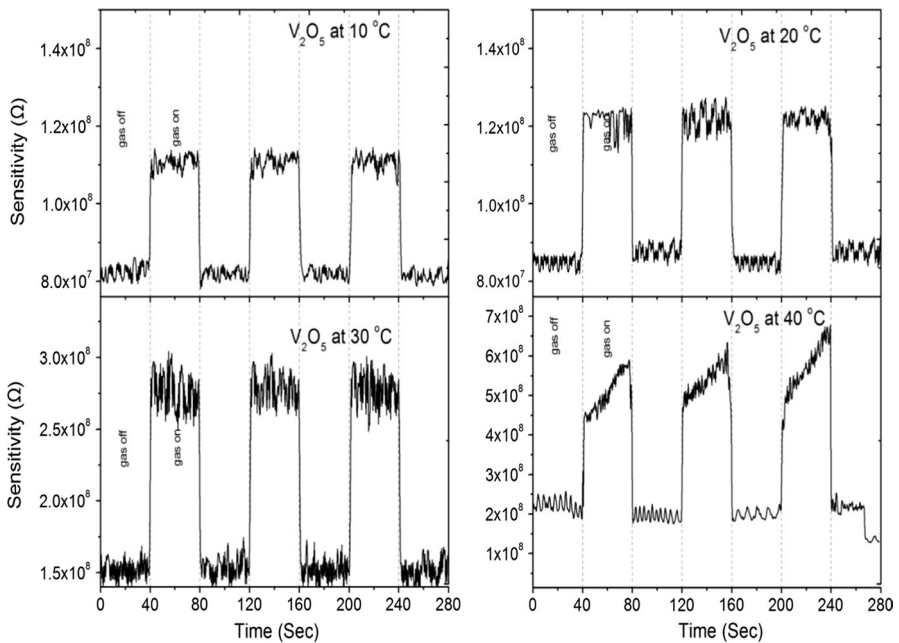| Film type	Response time (s)	Recovery time (s)
V_2O_5/MA	1.97	1.47
NiO/MA	8	0.77

Fig. 16 Sensing properties of the V_2O_5/PMA films at 10, 20, 30 and 40 °C
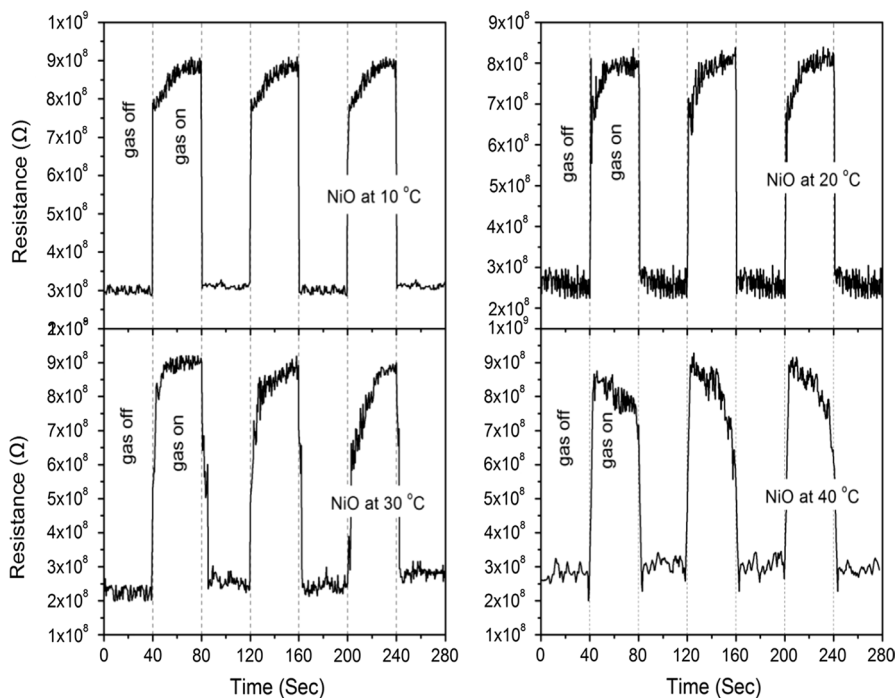
Fig. 17 Sensing properties of the NiO/PMA films at 10, 20, 30 and 40 °C
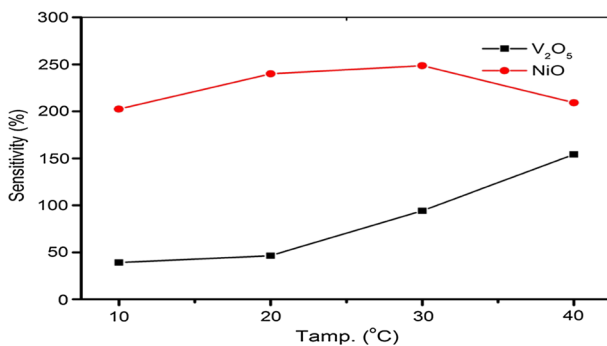

Fig. 18 Sensitivity of V_2O_5/PMA and NiO/PMA films with different temperatures

of N_2 gas (on–off) was 40 s. Only air was used in the case of gas off. In contrast, both air and N_2 have been utilized in the case of gas on (Fig. 18).

Table 8 shows the variation in both response and recovery times of V_2O_5/PMA and NiO/PMA films with different temperatures.

Table 8 Variation in both response and recovery times of V_2O_5/PMA and NiO/PMA films with different temperatures

Film type	T (°C)	Response time (s)	Recovery time (s)
V_2O_5/MA	10	4	1.3
	20	2.57	0.89
	30	2.2	0.77
	40	29.4	0.1
NiO/MA	10	12.32	0.37
	20	11.13	0.78
	30	14.5	3.5
	40	4.17	1.87

Conclusions

We have shown in this work that the PMA/V_2O_3 and PMA/$NiCl_2$ as nanocomposites were synthesized in a temperature-dependent manner. The grafting of a PMA chain into Fe_3O_4 and MO_x and the chain in thermal stability was shown by TG/DTG, DSC, XRD, AFM, FTIR, SEM, and FE-SEM measurements. Thermal analysis showed that the prepared nanocomposites were stable at temperature up to 500 °C. Both XRD powder pattern and AFM images were formed through a spinal crystal with crystalline sizes and particle sizes in the ranges of 10.9–40.13 nm and 72.12 and 88.12 nm, respectively. By contrast, SEM and FE-SEM images showed different forms of polymers with the cubic crystal structure of PMA/NiONC and Fe_3O_4 units, and orthorhombic crystal structure for PMA/VONC. Furthermore, the PMA/NiONC and PMA/VONC nanocomposites showed extremely good efficacy when applying gas sensitivity to N_2 gas and excellent efficacy for application of light detection.

References

1. Gupta PK, Hiremath L, Kumar SN, Srivastava AK, Shankarnarayan N, Vidyashree S, Singh SA (2017) Nanotechnology based sustained action drug delivery system: a review. Nanotechnology 5(4):20–32
2. Rogers B, Adams J, Pennathur S (2014) Nanotechnology: understanding small systems. CRC Press, London
3. Partizan G, Mansurov BZ, Medyanova BS, Koshanova AB, Mansurova ME, Aliyev BA, Jiang X (2016) Low-temperature synthesis of carbon nanotubes on iron nano powders. Mater Res Express 3(11):115010–115018
4. Duncan TV (2011) Applications of nanotechnology in food packaging and food safety: barrier materials, antimicrobials and sensors. J Colloid Interface Sci 363(1):1–24
5. Lyon D, Hubler A (2013) Gap size dependence of the dielectric strength in nano vacuum gaps. IEEE Trans Dielectr Electr Insul 20(4):1467–1471
6. Salim, M. T. M., "Synthesis of polymer nanocomposites based on organic polymers and inorganic nanostructures and their multifunctional applications ", Vol. 17 (4) 22–31 (2015)

7. Chowdhury, R. A "Review on the application of nanotechnology in pharmaceutical science", Doctoral dissertation, East West University, Vol.3 (3), 33 - 40 (2015)

8. Yang G, Zhu C, Du D, Zhu J, Lin Y (2015) Graphene-like two-dimensional layered nanomaterials: applications in biosensors and nanomedicine. Nano Scale 7(34):14217–14231

9. Laurent S, Forge D, Port M, Roch A, Robic C, Vander Elst L, Muller RN (2008) Magnetic iron oxide nanoparticles: synthesis, stabilization, vectorization, physicochemical characterizations, and biological applications. Chem Rev 108(6):2064–2110

10. Silva SR, Beliatis MJ, Jayawardena KD, Mills CA, Rhodes R, Rozanski LJ (2014) Hybrid and nanocomposite materials for flexible organic electronics applications. In: Handbook of flexible organic electronics: materials, manufacturing and applications, vol 57, pp 110–117

11. Jung HM, Kang JH, Yang SY, Won JC, Kim YS (2009) Barium titanate nanoparticles with diblock copolymer shielding layers for high-energy density nanocomposites. Chem Mater 22(2):450–456

12. Tchoul MN, Fillery SP, Koerner H, Drummy LF, Oyerokun FT, Mirau PA, Vaia RA (2010) Assemblies of titanium dioxide-polystyrene hybrid nanoparticles for dielectric applications. Chem Mater 22(5):1749–1759

13. Yang TI, Kofinas P (2007) Dielectric properties of polymer nanoparticle composites. Polymer 48(3):791–798

14. Stankic S, Suman S, Haque F, Vidic J (2016) Pure and multi metal oxide nanoparticles: synthesis, antibacterial and cytotoxic properties. J Nanobiotechnol 14(1):73–81

15. Kalantari K, Ahmad MB, Shameli K, Khandanlou R (2013) Synthesis of talc/Fe_3O_4 magnetic nanocomposites using chemical co-precipitation method. Int J Nanomed 8:1817–1824

16. Singh BP, Birendra P (2012) Synthesis and characterization of inorganic polymer nano- composites. Der Chem Sin 3(2):521–526

17. Zhang H, Hu Y, Wang Z, Fang Z, Peng L-M (2016) Performance boosting of flexible ZnO UV sensors with rational designed absorbing antireflection layer and humectant encapsulation. ACS Appl. Mater 8:381–389

18. Sadegh H, Shahryari-ghoshekandi R, Kazemi M (2014) Study in synthesis and characterization of carbon nanotubes decorated by magnetic iron oxide nanoparticles. Int Nano Lett 4(4):129–135

19. Zhao SB, Bilodeau E, Lemieux V, Beauchemin AM (2012) Hydrogen bonding directed intermolecular cope-type hydroamination of alkenes. Org Lett 14(19):5082–5085

20. Abbasi MA, Ibupoto ZH, Hussain M, Khan Y, Khan A, Nur O, Willander M (2012) Potentiometric zinc ion sensor based on honeycomb-like NiO nanostructures. Sensors 12(11):15424–15437

21. Oliveira M, Machado AV (2013) Preparation of polymer-based nanocomposites by different routes. In: Nanocomposites: synthesis, characterization and applications, pp 1–22

22. Birendrap S, Jai P, Shruti S (2012) Synthesis and characterization of inorganic nano-composites. Der chemical sinica 3(2):521–526

23. Nada MA, Safaa Z (2016) Synthesis and characterization of inorganic polymer nano composites from methyl acrylate and aluminum chloride and hexachloro palatinate (Iv). IJRPC 6(4):666–674

24. Rahman MR, Hamdan S (2017) Differential scanning calorimetry (DSC) and thermo gravimetric Analysis (TGA) of wood polymer nanocomposites. In: Mates web of conferences, vol 87, pp 22–30

25. Yang M, Dan Y (2006) Preparation of poly (methylmathacrylate)/titanium oxide composite particles via-situ emulsion polymerization. J Appl Polym Sci 101: 4056–4063

Publisher's Note Springer Nature remains neutral with regard to jurisdictional claims in published maps and institutional affiliations.